ACS APPLIED MATERIALS & INTERFACES

Research Article

www.acsami.org

Nanoplate-Built ZnO Hollow Microspheres Decorated with Gold Nanoparticles and Their Enhanced Photocatalytic and Gas-Sensing Properties

Weiwei Xia,[†,‡] Chao Mei,[†,‡] Xianghua Zeng,[*,‡] Guokang Fan,[§] Junfeng Lu,[⊥] Xiangdong Meng,[‡] and Xiaoshuang Shen[‡]

[‡]College of Physics Science and Technology & Institute of Optoelectronic Technology and [§]School of Chemistry and Chemical Engineering, Yangzhou University, Yangzhou 225002, P. R. China

[⊥]State Key Laboratory of Bioelectronics, School of Biological Science & Medical Engineering, Southeast University, Nanjing 210096, China

Supporting Information

ABSTRACT: Hierarchical porous ZnO microspheres decorated with gold nanoparticles (AuNPs) were successfully synthesized by a facile solvothermal route. The hierarchical ZnO superstructure was constructed of interconnected nanoplates with numerous voids. Photoluminescence, X-ray photoelectron spectroscopy, and electron paramagnetic resonance measurements demonstrated that the main defects were oxygen vacancies ($V_O^{\bullet}$) with minor interstitial oxygen (O_i^-) in the hierarchical ZnO hollow microspheres. The as-prepared hierarchical ZnO hollow microspheres and the AuNPs used to decorate them were examined for their photocatalytic degradation ability and as gas sensors. The photodegradation results demonstrated that the degradation rate constant on rhodamine B for undecorated ZnO microspheres was 0.43 min^{-1}, which increased to 1.76 min^{-1} for AuNP-decorated ZnO microspheres. The AuNP-functionalized ZnO microspheres displayed superior sensing properties, with a 3-fold enhancement in their gas response to 1 ppb of dibutyl phthalate.

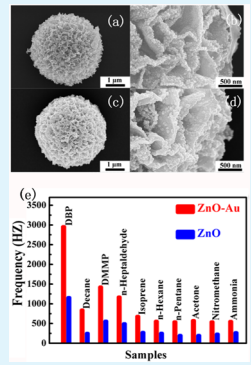

KEYWORDS: *ZnS, hollow microspheres, sensing properties, photocatalytic*

INTRODUCTION

With the increasing concern over safety in residential areas and environmental protection, the effective detection of toxic and hazardous gases, as well as the degradation of organic pollutants, has become imperative. As an important direct semiconductor with a band gap of 3.37 eV at 300 K and a large excitation binding energy of 60 meV, zinc oxide (ZnO) exhibits distinctive electrical, optical and electrochemical properties and can be applied in many fields of research, including solar cell,[1] catalytic support material,[2] transparent electrode[3] and semiconductor gas sensor[4] research. Nanostructured ZnO is generally considered a feasible candidate for use in photocatalysts and chemical sensors.[5] However, the development of high-performance photocatalysis and gas sensors remains a challenge. There are two common strategies that have been pursued in the literature to improve the properties of photocatalysts and gas sensors. One method is controlling the growth of nanomaterials with a specially designed size, shape, and morphology because the properties of photocatalysts and gas sensors are highly dependent on their surface-to-volume ratio. The other method is surface modification with noble metals, including silver, platinum (Pt), and gold (Au). In photocatalysis, photoinduced electrons and holes recombine quickly to decrease the available photocatalytic efficiency of ZnO, and noble metals can act as electron-scavenging centers to allow for effective electron−hole pair separation, leading to an enhancement in the photocatalytic activity.[6,7] Hence, the high performance of photocatalysts and gas sensors has motivated us to design ZnO materials with distinct morphologies. Furthermore, many efforts have been devoted to the preparation of various complex nanostructures of ZnO, including nanowires,[8] nanotubes,[9] porous nanoplates,[10] nanopyramids,[11] and hierarchical architectures.[12,13] Previous results have demonstrated that 3D hierarchical porous or hollow ZnO structures with large pores are highly advantageous for use in chemical sensors and photocatalysis because of their large surface area and facile mass transport in materials.[14−17] In particular, porous hollow ZnO microspheres have exhibited excellent sensor and photocatalysis performances because their loose porous-packed structure can provide a large surface area and a high density of active sites.[18] In addition, this unique structure demonstrates excellent incident light scattering within its interior and also facilitates gas diffusion and transport in sensing layers. Recently, people found that hydrogenated black ZnO nanoparticles demonstrated an enhanced photocatalytic

Received: February 10, 2015
Accepted: May 15, 2015
Published: May 15, 2015

DOI: 10.1021/acsami.5b01333
ACS Appl. Mater. Interfaces 2015, 7, 11824−11832

performance, which provides a new method to increase photocatalytic activities.[19]

Even though there is some work on the photocatalytic activities using Au/metal oxides as catalysts, for better applications in the future, we need rich raw materials as catalysts, a simple synthesized method, and a friendly environment; furthermore, the obtained catalysts can be reused many times. Therefore, much work needs to be done. For the Au/metal oxides, we should know how the morphology, size, and structure of the metal oxides, as well as the Au particle size, influence the photocatalytic activity.

In gas sensing, previous research has indicated that the incorporation of noble metals (Au, Pt, palladium, etc.) with semiconductor oxides by surface modification is an effective way to improve gas-sensing properties. The gas-sensing performance can be improved significantly because of the high catalytic activity of noble metals toward the test gases.[20−22] Although many studies on the development of photocatalysts and gas sensors using ZnO have been conducted, it remains a challenge to develop a facile and cost-effective procedure for producing such materials without using toxic reagents to design 3D hierarchical ZnO. Furthermore, Au nanoparticles (AuNPs) are incorporated into photocatalysts and gas-sensing materials because of their large surface-to-volume ratio and effective electron−hole pair separation.

In this study, we developed a facile two-stage solution process for successfully fabricating AuNP-functionalized monodispersed porous ZnO nanoplate-built hollow microspheres. Modified porous ZnO nanoplate-built hollow microspheres with AuNPs evenly distributed on their surface were synthesized by precipitating an aqueous solution of $HAuCl_4$ with sodium citrate. This green, nontoxic, and cost-effective procedure provides a general method for fabricating AuNP-modified metal oxide semiconductors. To demonstrate the practical applications of the synthesized material, the photocatalytic and gas-sensing performance of the as-fabricated AuNP-modified porous ZnO nanoplate-built hollow microspheres were systematically investigated. As expected, the microspheres displayed enhanced photocatalytic and gas-sensing performance relative to that of pure porous ZnO hollow microspheres. To the best of our knowledge, there are no reports on such a unique system that combines the advantages of porous ZnO nanoplate-built hollow microspheres and catalytic AuNPs. Our results demonstrate that the synthesized microspheres exhibit significantly enhanced photocatalytic and gas-sensing performance, which may provide a new pathway for the development of advanced materials of a similar type.

EXPERIMENTAL SECTION

Chemical reagents (analytical grade), namely, zinc acetate dihydrate [$Zn(CH_3COO)\cdot 2H_2O$], hexamethylenetetramine ($C_6H_{12}N_4$), sodium citrate ($C_6H_5Na_3O_7\cdot 2H_2O$), sodium hydroxide (NaOH), and chloroauric acid hydrate ($HAuCl_4\cdot 4H_2O$), were purchased from Sinopharm Chemical Reagent Co., Ltd., and used as received without further purification. Distilled water and absolute ethanol were used throughout the experiments.

Preparation of Porous ZnO Nanoplate-Built Hollow Microspheres. The details regarding the growth process of ZnO nanoplate-built hollow microspheres are similar to those reported in our previous study.[23] In a typical procedure, 10 mmol of $Zn(CH_3COO)\cdot 2H_2O$), 10 mmol of $C_6H_{12}N_4$, and 1 mmol of $C_6H_5Na_3O_7\cdot 2H_2O$ were dissolved in 100 mL of distilled water. The solution was then stirred for 30 min. The mixed solution was submitted to thermal treatment at 95 °C for 4 h. After the reaction, the solution was cooled to room temperature, and a white product was obtained after washing with distilled water and ethanol several times. Finally, the product was annealed at 400 °C for 30 min to yield crystalline porous ZnO hollow microspheres.

Preparation of ZnO Nanoparticles. ZnO nanoparticles were synthesized by a simple solvothermal method according to a previous report. In a typical procedure for the synthesis of ZnO nanoparticles, 1 mmol of $Zn(CH_3COO)\cdot 2H_2O$ and 5 mmol of NaOH were dissolved into 30 mL and agitated about 30 min. The mixture was transferred into a 50 mL stainless steel Teflon-lined autoclave and maintained at 160 °C for 24 h and finally cooled to room temperature naturally. The resulting product was collected by centrifugation, washed several times using distilled water and absolute ethanol, and dried in a vacuum stove at 60 °C for 10 h.

Nanoplate-Built ZnO Hollow Microspheres Decorated with AuNPs. The synthesis of decorated microspheres was performed according to a method reported in the literature with some modifications.[24] In a typical procedure, 40 mg of the as-prepared porous ZnO hollow microspheres was dispersed in 100 mL of distilled water mixed with 0.11 mL of $HAuCl_4$ (0.24 M) under stirring; the reaction solution was then heated to 110 °C. After stirring for 15 min, 3 mL of a 0.04 M $C_6H_5Na_3O_7$ solution was added to the mixture to reduce $HAuCl_4$ to metallic AuNPs. After stirring for approximately 40 min, a pink precipitate was obtained by centrifugation, washed several times using distilled water and absolute ethanol, and dried in a vacuum stove at 60 °C for 12 h. A change in the color of the pristine ZnO microspheres from white to pink indicated that AuNPs were successfully decorated on the microstructures.

Characterization. X-ray diffraction (XRD) analysis for phase identification was performed using a Bruker D8 advance diffractometer with Cu Kα radiation (λ = 1.5406 Å). The morphology and microstructure of the obtained products were characterized by a Hitachi S-4800 field-emission scanning electron microscope and a Tecnai G2 F30 field-emission transmission electron microscope with an accelerating voltage of 300 kV, respectively. Electron paramagnetic resonance (EPR) data of the samples were obtained using an ESRA-300 spectrometer. Photoluminescence (PL) measurements were performed on a Hitachi F-4600 fluorescence spectrometer using a 150 W xenon lamp (excitation wavelength: 340 nm) at room temperature. X-ray photoelectron spectroscopy (XPS) analysis was conducted on an ESCALAB-250Xi photoelectron spectrometer at 1.2 × 10^{-9} mbar using an Al Kα X-ray beam (1486.6 eV). The XPS spectra were charge-corrected to the adventitious C 1s peak at 284.6 eV. UV−vis spectra were measured on a UV−vis−near-IR spectrometer (Cary-5000, Varian).

Photocatalytic Activity Measurement. The photocatalytic performance of the as-prepared samples was evaluated by decomposing the model pollutants rhodamine B (RhB) and methyl orange (MO) under UV-light irradiation at room temperature. The photocatalytic reaction was performed as follows: 40 mg of as-prepared samples was suspended in separate 100 mL aqueous solutions of RhB and MO (100 mL, 1 × 10^{-5} mol/L). Prior to visible-light irradiation, the suspensions were sonicated for 10 min and then magnetically stirred in the dark for 30 min to obtain desorption−adsorption equilibrium. The solutions were then exposed to UV-light irradiation. Samples of 5 mL were collected after a period of 10 min and then centrifuged to remove the residual photocatalyst. The clear supernatant was then analyzed by recording the maximum absorption band using a Shimadzu UV-3600 spectrophotometer. Comparative experiments of the degradation of RhB by using ZnO nanoparticles and commercial TiO_2 (P-25) powders were also carried out.

Gas-Sensing Experiment. Gas sensors based on the as-prepared products were examined using the quartz crystal microbalance (QCM) technique.[25] A QCM measures the mass attributed to analyte binding by measuring the change in frequency of a quartz crystal resonator. The gas-sensing response was measured in a 500 mL sealed chamber. A coated quartz crystal served as the sensing QCM, and another noncoated one was the reference sample. The frequency difference between the two was recorded every second by a computer. The change in frequency was recorded as soon as a gas sample, such as

DOI: 10.1021/acsami.5b01333
ACS Appl. Mater. Interfaces 2015, 7, 11824−11832

dimethyl methylphosphonate (DMMP), was injected into the chamber. A more detailed description can be found in the aforementioned paper.[26]

RESULTS AND DISCUSSION

The crystalline structures of pristine ZnO microspheres and those decorated with AuNPs were identified from the XRD patterns. Figure 1a shows the XRD patterns of the pristine

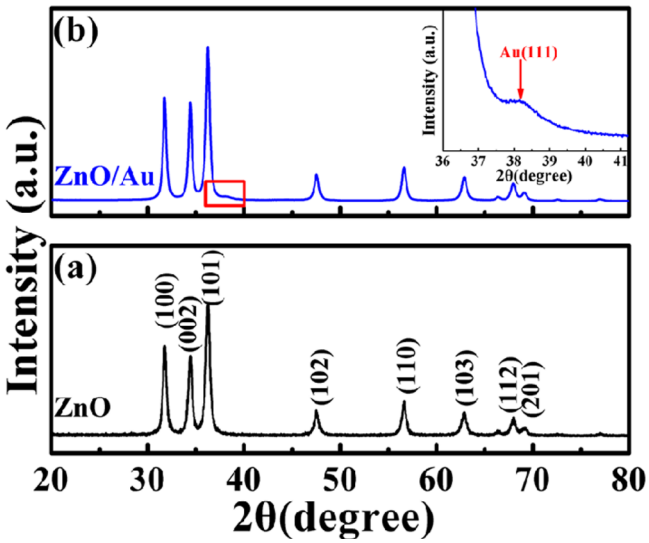

Figure 1. XRD patterns of crystalline ZnO (a) and AuNP-decorated ZnO (b). The inset of part b shows a magnification of the pattern at 2θ values ranging from 36° to 41° for AuNP-decorated ZnO.

porous ZnO hollow microspheres. The figure indicates that the main reflection peaks match well with the standard data of the wurtzite structure of ZnO (JCPDS card no. 36-1451), with a = 3.25 Å and c = 5.21 Å. No extra peak was detected by XRD, indicating the superior purity of the ZnO product. As shown in Figure 1b, for the AuNP-decorated porous ZnO hollow microspheres, in addition to the pure ZnO peaks, an extra weak peak at 2θ = 38.2° is observed, which corresponds to the (111) planes of face-centered-cubic Au (JCPDS card no. 01-1174). The weak diffraction peak for Au implies a low content of Au in the final product.[27]

The morphologies of the as-prepared ZnO microspheres and those decorated with AuNPs were examined by scanning electron microscopy (SEM) measurements. The low-magnification SEM image shows that a single hierarchical ZnO microsphere had a diameter of 2−3 μm (Figure 2a). By close observation of the high-magnification SEM image in Figure 2b, it can be concluded that the hierarchical ZnO microsphere was formed by the self-assembly of many nanoplates, with each nanoplate possessing a thickness of tens of nanometers; moreover, on the surface of the microsphere, the separation between two adjacent nanoplates can be observed to be on the order of approximately several hundreds of nanometers. Figure 2c displays an SEM image of a ZnO microsphere decorated with AuNPs. By comparison of the images before and after decoration, it can be observed that the overall morphology of the ZnO microsphere was inherited. Figure 2d reveals a typical magnified SEM image of the nanoplates decorated with AuNPs, demonstrating that AuNPs measuring several tens of nanometers were uniformly distributed on the surface of the ZnO nanoplates. SEM elemental mappings were conducted to

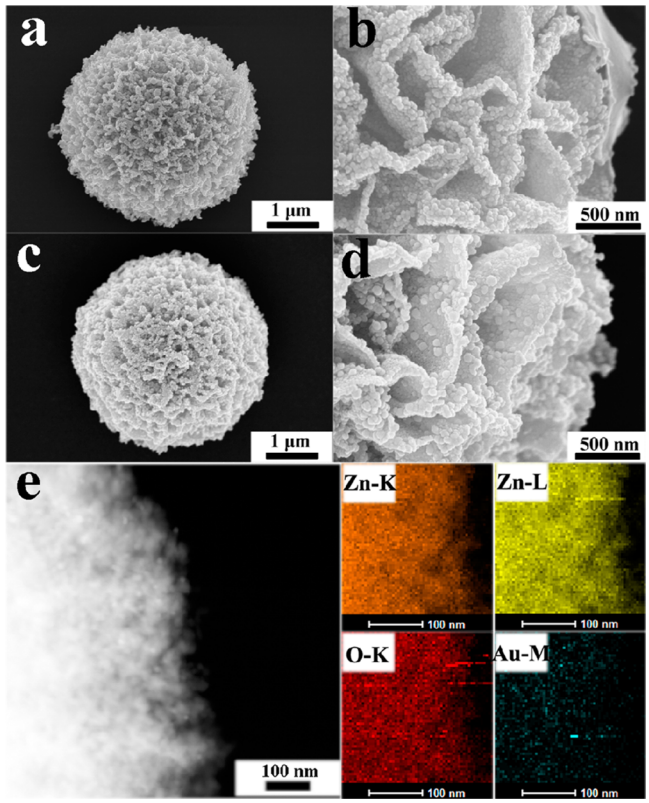

Figure 2. (a) Low-magnification SEM image of a single hierarchical ZnO microsphere composed of nanoplate building blocks. (b) Magnified SEM image showing the network character of the nanoplates. (c) Low-magnification SEM image of a single hierarchical ZnO microsphere decorated with AuNPs. (d) Magnified SEM image showing the network character of nanoplates loaded with AuNPs. (e) Elemental mappings of a ZnO microsphere decorated with AuNPs.

determine the spatial distribution of zinc (Zn), oxygen (O), and Au in the ZnO microsphere (Figure 2e). It can be confirmed that AuNPs were distributed homogeneously throughout the entire ZnO microsphere.

To obtain detailed information about the microstructures of pure ZnO microspheres and those decorated with AuNPs, we carried out high-reolsution transmission elelctron microscopy (HRTEM) measurements; the corresponding images are shown in Figure 3. In parts a and b of Figure 3, as-prepared ZnO microspheres with many mesopores can be observed to have been composed of many nanosheets, and a separation distance of several tens of nanometers can be observed between the nanosheets, which is consistent with the SEM images. Furthermore, HRTEM images were captured to study the surface microstructure of the ZnO nanoplates. As shown in Figure 3c, the measured d spacings of 0.16 and 0.26 nm correspond to the (110) and (002) crystal planes of ZnO (JCPDS card no. 36-1451), respectively. On the other hand, Figure 3b displays a low-magnification TEM image of ZnO microspheres decorated with AuNPs. Figure 3d further confirms the presence of both ZnO and AuNPs because the measured d spacings of 0.23 and 0.19 nm correspond to the (111) plane of the AuNPs and the (102) plane of ZnO, respectively.

As-prepared hollow ZnO microspheres with a high surface area would typically lead to high surface defect density. It has been demonstrated that surface defects have become

DOI: 10.1021/acsami.5b01333
ACS Appl. Mater. Interfaces 2015, 7, 11824−11832

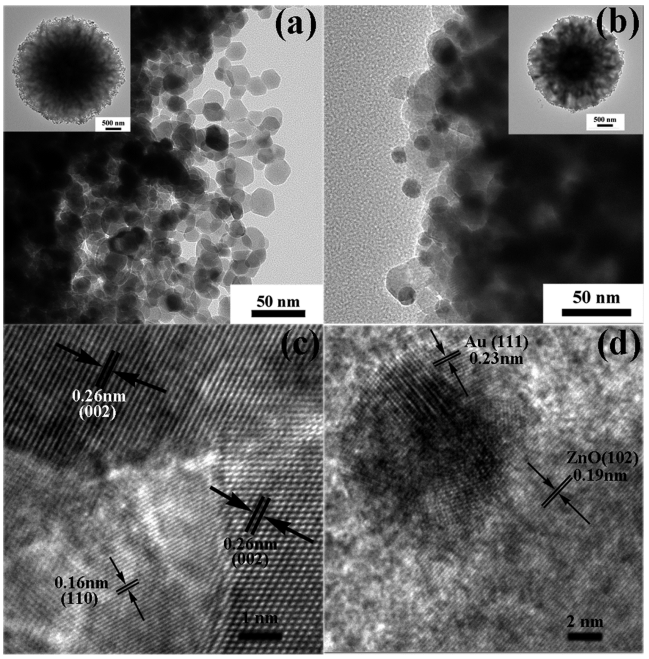

Figure 3. (a) TEM image of the surface of ZnO microspheres. Inset: TEM image of an individual hollow ZnO microsphere. (b) TEM image of the surface of ZnO microspheres decorated with AuNPs. Inset: TEM image of an individual hollow ZnO microsphere decorated with AuNPs. (c) HRTEM image showing the surface of a ZnO microsphere. (d) HRTEM image of a single AuNP attached to the surface of a ZnO microsphere.

increasingly important in determining the properties of photocatalysts and gas-sensing materials.[28] EPR and XPS are useful tools for monitoring the various behaviors of native defects, such as vacancies and interstitials. To identify the intrinsic defects in ZnO microspheres, we carried out XPS measurements. As shown in the survey XPS spectrum in Figure 4a, the Zn $2p_{3/2}$ peak at 1021.2 eV and the O 1s peak at 530.3 eV can be assigned to the elemental Zn and O in ZnO, respectively. Figure 4b presents the high-resolution spectrum of Zn 2p, and the peak positions of Zn $2p_{1/2}$ and Zn $2p_{3/2}$ are located at 1044.4 and 1021.2 eV, respectively. It can be concluded that the elemental Zn in the as-prepared ZnO microspheres was in the Zn^{2+} state, and no metallic Zn was detected. In addition, on the basis of the XPS results (see Table S1 in the Supporting Information, SI), the atomic concentration ratio of surface Zn to O was approximately 1.11, indicating an oxygen deficiency. The high-resolution spectrum of O 1s is illustrated in Figure 4c. The O 1s spectrum can be fitted with three energy components, a low-binding-energy peak (LP), a middle-binding-energy peak (MP), and a high-binding-energy peak (HP) located at 530.15, 531.50, and 532.28 eV, respectively, consistent with previously reported work.[29] The MP peak is typically assigned to O^{2-} ions in the oxygen-deficient regions ($V_O^{\bullet}$), and the LP peak can be attributed to O^{2-} ions at interstitial sites in the ZnO structure (O_i^{-}). In addition, the HP peak at 532.28 eV can be attributed to chemisorbed O.[30] To further confirm the existence of defects, EPR analysis of the ZnO microspheres was performed at room temperature, the results of which are shown in Figure 4d. The aforementioned defects, vacancies, and interstitials with unpaired electrons were paramagnetic in nature and were responsible for generation of the EPR signals. Although the existence of defect-related paramagnetic centers is still highly controversial, there are four types of lattice defects in microcrystalline ZnO that can be identified based on previous studies on EPR responses from ZnO: V_{Zn} (Zn vacancies), Zn_i (Zn at interstitial sites), O_i (O at interstitial sites), and three types of O vacancies (V_O^{++}, V_O^{+}, V_O).[31] Pristine ZnO showed a broad signal at $g \approx 1.9629$ and a sharp signal at $g \approx 2.0058$. On the basis of previous reports, the signal at $g \approx 1.9629$ is attributed to different defects such as $V_O^{\bullet}$[27] and Zn_i,[32,33] and the signal at $g \approx 2.0058$ is commonly attributed to V_{Zn} and O_i^{-}.[34−36] However, in our case, Zn vacancies and interstitials were not detected based on the XPS results shown in Figure 4b.

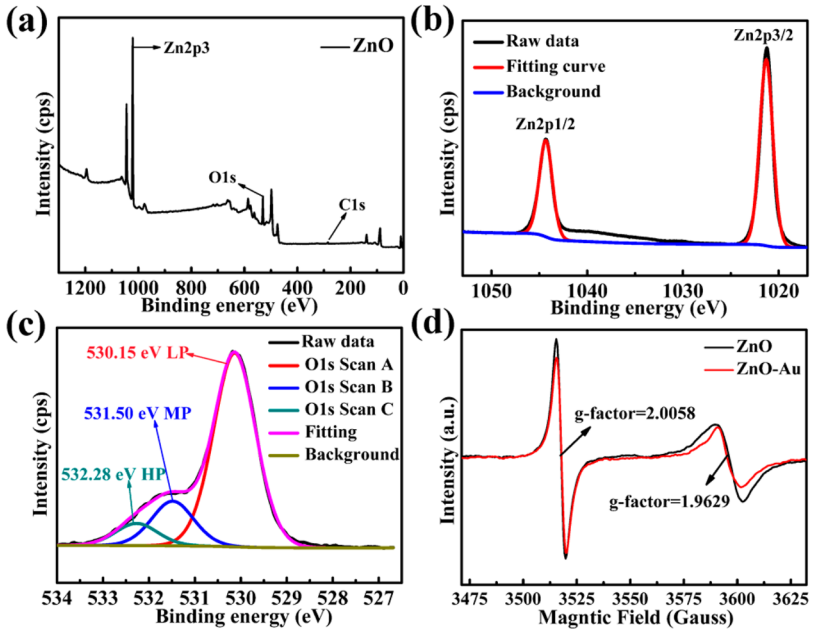

Figure 4. (a) Survey XPS spectrum of ZnO. (b) High-resolution Zn 2p spectrum. (c) High-resolution O 1s spectrum. (d) EPR spectra of ZnO and AuNP-decorated ZnO. The g factor can be calculated by the equation $g = h\nu/\mu_B B$.

DOI: 10.1021/acsami.5b01333
ACS Appl. Mater. Interfaces 2015, 7, 11824−11832

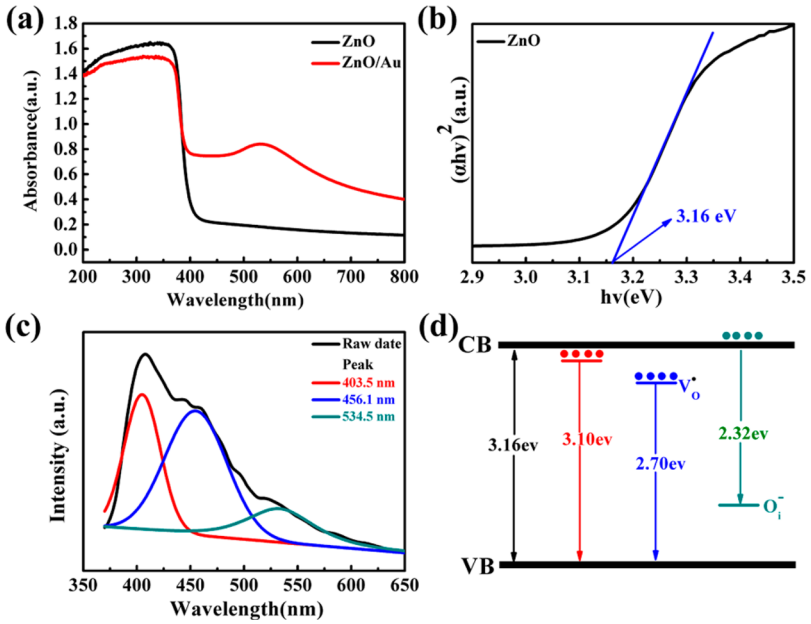

Figure 5. (a) UV−vis spectra of ZnO and AuNP-decorated ZnO. (b) Plots of $(\alpha h\nu)^2$ versus photon energy $(h\nu)$ for as-prepared ZnO microspheres. (c) Gaussian fit of the PL spectrum of ZnO microspheres with excitation at 340 nm. (d) Schematic diagram of the energy band of ZnO microspheres: CB, conduction band; VB, valence band; O_i^-, single interstitial oxygen ion; $V_O^\bullet$, single ionized oxygen vacancy.

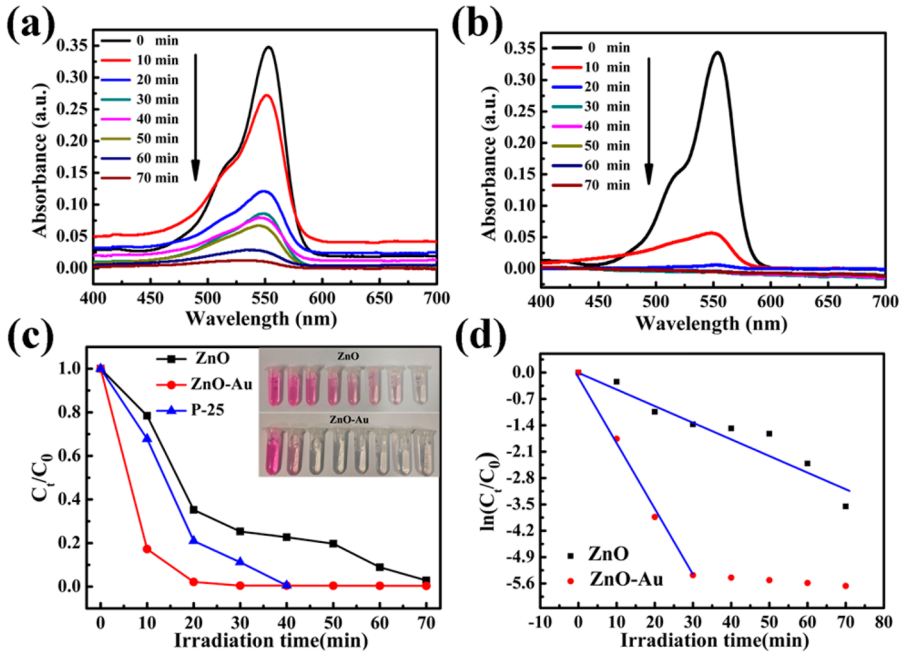

Figure 6. Absorption spectra of a RhB solution as a function of the UV irradiation time in the presence of (a) ZnO and (b) AuNP-decorated ZnO. (c) Comparison of the photocatalytic degradation of RhB in the presence of ZnO, AuNP-decorated ZnO, and commercial TiO_2. (d) Logarithm of the normalized concentrations as a function of the UV irradiation time for the RhB solution in the presence of ZnO and AuNP-decorated ZnO. The inset is a photograph of the color change of RhB during the photodegradation process.

In this case, we are inclined to attribute the ESR signals at $g \approx 1.9629$ and 2.0058 to $V_O^\bullet$ and O_i^-, respectively. In addition, density functional theory calculations suggest the existence of $V_O^\bullet$ and O_i^-.[37]

To test our hypothesis concerning the presence of defect-related paramagnetic centers, UV−vis and PL measurements were performed to determine the defect energy levels in the band gap of the as-prepared ZnO microspheres. Figure 5a shows the UV−vis absorption spectra of pure ZnO microspheres and those decorated with AuNPs. In addition to the UV absorption peak of ZnO at 373 nm, a surface plasma resonance peak of AuNPs is observed at ∼550 nm. A plot of $(\alpha h\nu)^2$ versus photon energy $(h\nu)$ is shown in Figure 5b to estimate the optical band gap of ZnO by the following equation:[38]

$$\alpha h\nu = C(h\nu - E_g)^{1/2} \quad (1)$$

where C is the parameter associated with the effective masses of electrons in the valence (VB) and conduction (CB) bands and

DOI: 10.1021/acsami.5b01333
ACS Appl. Mater. Interfaces 2015, 7, 11824−11832

$h\nu$ is the photon energy. For the pure ZnO microspheres, a band gap value of 3.16 was obtained based on the intersection points of the linear fit of the absorption spectra with the energy axis, as shown in Figure 5a,b.

The room temperature PL spectrum exhibits a broad peak, and multipeak Gaussian-fitting emission bands are observed at 403.5 nm (3.10 eV), 456.1 nm (2.72 eV), and 534.5 nm (2.32 eV). The emission band at 403.5 nm (3.10 eV) can be ascribed to the band edge or excitonic emission, with a Stokes shift of approximately 60 meV due to electron−phonon coupling. The peak centered at 456.1 nm can be assigned to $V_O^{\bullet}$ centers and to VB emission.[39,40] The yellow luminescence observed, with the peak centered at 534.5 nm, can be ascribed to the optical transition of photogenerated electrons from the CB to O_i^- centers.[41] On the basis of the above-described experimental results and theoretical analysis, the energy band structure diagram shown in Figure 5d was proposed for the as-prepared ZnO microspheres.

To explore the effect of surface modification with AuNPs on dye degradation, two model pollutants, RhB and MO, were used. The photocatalytic activities of the ZnO and AuNP-decorated ZnO structures toward the degradation of RhB under UV-light irradiation are shown in Figure 6. The typical time evolution of the absorption spectra of RhB after photodegradation by the ZnO and AuNP-decorated ZnO microspheres is depicted in Figure 6a,b. With increasing time, the intensity of the peak at 554 nm decreased gradually, which indicates that RhB was gradually photodegraded. The degradation efficiency is defined as C/C_0, where C_0 is the initial concentration and C is the concentration during the reaction. The degradation efficiencies of the pure ZnO microspheres, AuNP-decorated ZnO microspheres, and commercial TiO_2 are shown in Figure 6c, which clearly reveal that ZnO decorated with AuNPs exhibited better catalytic degradation than the pure ZnO microspheres did. It is worth mentioning that AuNP-decorated ZnO microspheres exhibited a better catalytic degradation of RhB than commercial TiO_2. Under UV illumination for approximately 20 min, the ZnO microspheres decorated with AuNPs could successfully degrade up to 98% of the RhB dye. On the other hand, for pure ZnO microspheres, 97% degradation could be achieved for an exposure duration of 70 min. The enhanced degradation of the dye is attributed to large surface states, consistent with previously reported results.[42] The inset photographs in Figure 6c show the corresponding color changes of the RhB solutions with increasing reaction time. It can be clearly seen from the result of the comparative experiment that nanoplate-built ZnO hollow microspheres exhibit superior photocatalytic activity compared to ZnO nanoparticles. Such excellent photocatalytic activities can be attributed to the novel nanoplate-built ZnO microspheres.

Moreover, it was observed that degradation of the dyes followed a first-order rate law by linear transformation of the following equation:[43]

$$\ln(C_0/C_t) = kt \tag{2}$$

The corresponding kinetic plots are presented in Figure 6d. The degradation rate constants k were calculated to be 1.76 and 0.43 min^{-1} for the pure ZnO and AuNP-decorated ZnO microspheres, respectively.

In comparison with the photocatalytic activities of ordinary ZnO nanoparticles, the ZnO nanoparticles were synthesized and conducted for the degradation of RhB under UV irradiation (see Figure S1 in the SI). Figure S1a in the SI is the SEM image of the as-synthesized ZnO nanoparticles, and Figure S1b in the SI contains the adsorption spectra of RhB solutions in the presence of ZnO nanoparticles under UV light at different periods of time. The logarithm of the normalized concentrations as a function of the UV irradiation time with ZnO microspheres and ZnO nanoparticles as catalysts on the degradation of RhB solutions revealed that the ZnO microspheres have better photocatalytic activities than the ZnO nanoparticles, as shown in Figure S1c in the SI. To evaluate the stability and reusability of the photocatalytic activity, the AuNP-decorated ZnO microspheres were used to degrade RhB dye in five repeated cycles; as displayed in Figure S1d in the SI, the photocatalytic activity can be well retained because there is only 7% reduction after five cycling runs. Such favorable photostability may be ascribed to the excellent structural stability of nanoplate-built ZnO hollow microspheres. It can be observed that the nanoplate-built ZnO hollow microspheres still kept the original structure, and the AuNPs attached firmly on the surface of the ZnO nanoplates after being used five times (see Figure S2 in the SI). Similar kinetics and rate constant values were observed for the degradation of MO by ZnO and AuNP-decorated ZnO, as shown in Figure S3 in the SI. The above-described results demonstrate that AuNPs can greatly improve the photocatalytic properties of the nanoplate-built ZnO microspheres, in good agreement with the reported literature.[2,44]

The photocatalytic degradation mechanism of RhB in the presence of ZnO microspheres is as follows. First, the photons with energies greater than or equal to the band-gap energy of the photocatalyst are absorbed onto the nanospheres' surface, resulting in the formation of holes (h_{VB}^+) in the VB and an electron (e_{CB}^-) in the CB, as listed in eq 5. Then, the holes h_{VB}^+ will react with water or hydroxyl groups to generate $^{\bullet}OH$ (eqs 4 and 5). Finally, hydroxyl radical $^{\bullet}OH$ can react with RhB molecules to exert the degradation of RhB (eq 6).

$$ZnO + h\nu \rightarrow ZnO\ (e_{CB}^- + h_{VB}^+) \tag{3}$$

$$h_{VB}^+ + H_2O \rightarrow H^+ + {}^{\bullet}OH \tag{4}$$

$$h_{VB}^+ + OH^- \rightarrow {}^{\bullet}OH \tag{5}$$

$$^{\bullet}OH + RhB \rightarrow H_2O + CO_2 \tag{6}$$

Here, the much better photocatalytic activities for the porous ZnO microspheres than for the normal ZnO materials can be ascribed to the large specific surface areas. To compare the specific surface areas of hierachical ZnO microspheres and nanoparticles, we have carried out the specific surface area measurements by nitrogen adsorption−desorption isotherms, as shown in Figure S4 in the SI, and it shows that the specific surface area of the ZnO nanoplate-built hollow microspheres is 44.26 m^2/g, which is more than 20% larger than the value of 34.83 m^2/g for ZnO nanoparticles. Hence, the ZnO microspheres with a large specific surface area can adsorb more pollutant molecules and light,[45] which will be beneficial to the degradation of RhB, resulting in better photocatalytic activity than that of the same material with a smaller specific surface area. For the Au-decorated ZnO microspheres, the enhanced catalytic activity can be explained as first Au-decorated ZnO microspheres were excited by UV light with photons, leading to the generation of electrons in the semiconductor CB and electron holes in the VB; then, because of the existence of

DOI: 10.1021/acsami.5b01333
ACS Appl. Mater. Interfaces 2015, 7, 11824−11832

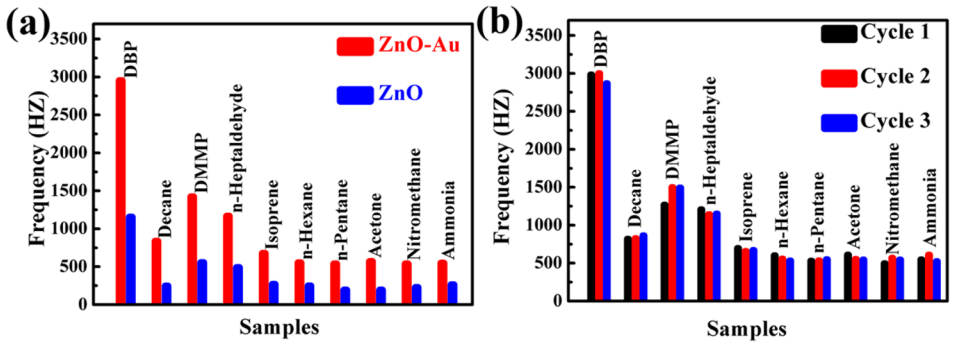

Figure 7. (a) Gas-sensing performance of pure ZnO microspheres and AuNP-decorated ZnO with respect to different gases. (b) Reproducibility of the performance of a AuNP-functionalized ZnO sensor over three cycles.

AuNPs, the ZnO microspheres have a wide absorption band approximately at 550 nm (as shown in Figure 5a), so the photoinduced electron in the CB would transfer to AuNPs acting as an electron buffer, which can hinder electron−hole pair recombination. The long-lived electron−hole pairs are prone to generate a larger amount of photoreactive species, which may account for the higher photocatalytic activity of the Au-decorated ZnO composites than that of bare ZnO nanoparticles. So, the adsorption of Au on the surface of ZnO mircospheres can greatly improve the photocatalytic activity by preventing the holes from attacking the surface O of ZnO and inhibiting the photocorrosion effect.[46]

We further investigated the effects of AuNP decoration on the gas-sensing performance of ZnO microspheres; the test results are presented in Figure 7. Several conventional volatile organic vapors were tested, namely, dibutyl phthalate (DBP), decane, DMMP, *n*-heptaldehyde, isoprene, *n*-hexane, *n*-pentane, acetone, nitromethane, and ammonia. The test results indicate that the sensors based on the two types of microstructures were more sensitive to DBP vapor than to the other volatile organic vapors. Figure 7a clearly shows that the sensor based on AuNP-functionalized ZnO microspheres exhibited extraordinarily higher sensitivity than did the pristine ZnO sensor. The AuNP-decorated ZnO sensor showed the highest response (2952 Hz) to a very low concentration (1 ppb) of DBP, indicating ppb-level detection of DBP. Reproducibility is also an important property of a chemical sensor. Thus, we also examined the response of the AuNP-functionalized ZnO sensor over three cycles. The results, as shown in Figure 7b, demonstrate that the AuNP-functionalized ZnO sensor exhibited good stability because no distinct changes in the response amplitude could be observed. The above-described results strongly suggest that the as-prepared hierarchical Au-decorated porous ZnO microspheres are a promising candidate for gas-sensing applications.

In summary, AuNP-functionalized ZnO microspheres show significantly enhanced photocatalytic and gas-sensing performance. Several possible reasons may be responsible for this improved performance. First, the unique porous ZnO nanoplate-built hollow microspheres could provide a large surface area with more reactive sites and high surface accessibility. Additionally, the voids and interspaces among the interconnected ZnO nanosheets also largely facilitated incident light scattering within the structures and also provided a facile route for gas diffusion and transport in the sensing layers. Second, during photocatalysis, the charge-transfer processes occur at the surface of the AuNPs and at the interface of the ZnO nanosheets, which is crucial for optimizing the performance of AuNP-functionalized ZnO catalysts. In gas sensing, the incorporation of AuNPs into porous ZnO nanosheets can enrich the ion sorption of O species (O_2^-, O^-, and O^{2-}), enhancing the extent of reaction due to the well-known spillover effect.[47] In addition, AuNP-functionalized ZnO microspheres can also provide a large surface area, which is advantageous for producing highly responsive gas sensors. The reason for the good selectivity observed is not clear at the moment. Further research is needed to gain a deeper understanding of the selectivity behavior. This work is currently underway.

CONCLUSIONS

In this study, self-assembled hierarchical ZnO hollow microspheres were successfully prepared by a simple hydrothermal process followed by calcination. The ZnO hollow microspheres were composed of single-crystalline porous interconnected nanoplates with an abundance of uniformly distributed voids. AuNPs were decorated on the surface of the ZnO hollow microspheres via a facile aqueous solution method. XRD and HRTEM analyses showed that the ZnO hollow microspheres were polycrystalline with a wurtzite structure (JCPDS card no. 36-1451). On the basis of the experimental results (PL, EPR, and XPS) and theoretical analysis, the primary defects in the ZnO hollow microspheres were $V_O^{\bullet}$ and O_i^-. Photodegradation tests using RhB and MO dyes in the presence of UV light revealed a drastic improvement in the catalytic efficiency after the introduction of AuNPs. Both pure ZnO and AuNP-functionalized ZnO microspheres were incorporated into gas-sensing devices to determine the effects of AuNPs on the sensing performance. The results show that ZnO hollow microspheres decorated with AuNPs exhibit gas-sensing properties superior to those of undecorated microspheres with respect to sensitivity and stability. The above-described results should be of great significance to fields related to energy and the environment from scientific and engineering viewpoints.

ASSOCIATED CONTENT

Supporting Information

Table of surface atomic concentrations, SEM images, absorption spectra, nitrogen adsorption−desorption isotherms, photocatalytic degradation, and logarithms of the normalized concentrations. The Supporting Information is available free of charge on the ACS Publications website at DOI: 10.1021/acsami.5b01333.

DOI: 10.1021/acsami.5b01333
ACS Appl. Mater. Interfaces 2015, 7, 11824−11832

AUTHOR INFORMATION

Corresponding Author

*E-mail: xhzeng@yzu.edu.cn.

Author Contributions

†These authors contributed equally to this work.

Notes

The authors declare no competing financial interest.

ACKNOWLEDGMENTS

We gratefully acknowledge financial support for this work from the National Natural Science Foundation of China (Grant 61474096), the Natural Science Foundation of the Higher Education Institutions of Jiangsu Province, China (Grant 14KJB510036), and the Science and Technology Innovation Cultivation Fund of Yangzhou University (Grant 2014CXJ013).

REFERENCES

(1) Kim, H.; Jeong, H.; An, T. K.; Park, C. E.; Yong, K. Hybrid-Type Quantum-Dot Cosensitized ZnO Nanowire Solar Cell with Enhanced Visible-Light Harvesting. *ACS Appl. Mater. Interfaces* **2013**, *5*, 268−275.

(2) Udawatte, N.; Lee, M.; Kim, J.; Lee, D. Well-Defined Au/ZnO Nanoparticle Composites Exhibiting Enhanced Photocatalytic Activities. *ACS Appl. Mater. Interfaces* **2011**, *3*, 4531−4538.

(3) Ko, Y. H.; Nagaraju, G.; Lee, S. H.; Yu, J. S. PDMS-based Triboelectric and Transparent Nanogenerators with ZnO Nanorod Arrays. *ACS Appl. Mater. Interfaces* **2014**, *6*, 6631−6637.

(4) Kim, J.; Yong, K. Mechanism Study of ZnO Nanorod-Bundle Sensors for H_2S Gas Sensing. *J. Phys. Chem. C* **2011**, *115*, 7218−7224.

(5) Wang, Z. L. Splendid One-Dimensional Nanostructures of Zinc Oxide: A New Nanomaterial Family for Nanotechnology. *ACS Nano* **2008**, *2*, 1987−1992.

(6) Chang, Y. G.; Xu, J.; Zhang, Y. Y.; Ma, S. Y.; Xin, L. H.; Zhu, L.N.; Xu, C. T. Optical Properties and Photocatalytic Performances of Pd Modified ZnO Samples. *J. Phys. Chem. C* **2009**, *113*, 18761−18767.

(7) Georgekutty, R.; Seery, M. K.; Pillai, S. C. A Highly Efficient Ag-ZnO Photocatalyst: Synthesis, Properties, and Mechanism. *J. Phys. Chem. C* **2008**, *112*, 13563−13570.

(8) Park, S.; An, S.; Ko, H.; Jin, C.; Lee, C. Synthesis of Nanograined ZnO Nanowires and Their Enhanced Gas Sensing Properties. *ACS Appl. Mater. Interfaces* **2012**, *4*, 3650−3656.

(9) Xiao, F. X. Construction of Highly Ordered ZnO−TiO_2 Nanotube Arrays (ZnO/TNTs) Heterostructure for Photocatalytic Application. *ACS Appl. Mater. Interfaces* **2012**, *4*, 7055−7063.

(10) Yu, J. C.; Xu, A. W.; Zhang, L. Z.; Song, R. Q.; Wu, L. Synthesis and Characterization of Porous Magnesium Hydroxide and Oxide Nanoplates. *J. Phys. Chem. B* **2004**, *108*, 64−70.

(11) Li, P.; Wei, Z.; Wu, T.; Peng, Q.; Li, Y. D. Au−ZnO Hybrid Nanopyramids and Their Photocatalytic Properties. *J. Am. Chem. Soc.* **2011**, *133*, 5660−5663.

(12) Zhang, D. F.; Sun, L. D.; Zhang, J.; Yan, Z. G.; Yan, C. H. Hierarchical Construction of ZnO Architectures Promoted by Heterogeneous Nucleation. *Cryst. Growth Des.* **2008**, *8*, 3609−3615.

(13) Wu, Q. Z.; Chen, X.; Zhang, P.; Han, Y. C.; Chen, X. M.; Yan, Y. H.; Li, S. P. Amino Acid-Assisted Synthesis of ZnO Hierarchical Architectures and Their Novel Photocatalytic Activities. *Cryst. Growth Des.* **2008**, *8*, 3010−3018.

(14) Li, J.; Fan, H. Q.; Jia, X. H. Multilayered ZnO Nanosheets with 3D Porous Architectures: Synthesis and Gas Sensing Application. *J. Phys. Chem. C* **2010**, *114*, 14684−14691.

(15) Fan, F. Y.; Feng, Y. J.; Tang, P. G.; Chen, A. F.; Luo, R. X.; Li, D. Q. Synthesis and Gas Sensing Performance of Dandelion-Like ZnO with Hierarchical Porous Structure. *Ind. Eng. Chem. Res.* **2014**, *53*, 12737−12743.

(16) Wang, X. Z.; Liu, W.; Liu, J. G.; Wang, F. L.; Kong, J.; Qiu, S.; He, C. Z.; Luan, L. Q. Synthesis of Nestlike ZnO Hierarchically Porous Structures and Analysis of Their Gas Sensing Properties. *ACS Appl. Mater. Interfaces* **2012**, *4*, 817−825.

(17) Zhang, J.; Wang, S. R.; Xu, M. J.; Wang, Y.; Zhu, B. L.; Zhang, S. M.; Huang, W. P.; Wu, S. H. Hierarchically Porous ZnO Architectures for Gas Sensor Application. *Cryst. Growth Des.* **2009**, *9*, 3532−3537.

(18) Zeng, H. B.; Cai, W. P.; Liu, P. S.; Xu, X. X.; Zhou, H. J.; Klingshirn, C.; Kalt, H. ZnO-based Hollow Nanoparticles by Selective Etching: Elimination and Reconstruction of Metal-semiconductor Interface, Improvement of Blue Emission and Photocatalysis. *ACS Nano* **2008**, *2*, 1661−1670.

(19) Xia, T.; Wallenmeyer, P.; Anderson, A.; Murowchick, J.; Liu, L.; Chen, X. B. Hydrogenated black ZnO nanoparticles with enhanced photocatalytic performance. *RSC Adv.* **2014**, *4*, 41654−41658.

(20) Yao, K. X.; Zeng, H. C. Fabrication and Surface Properties of Composite Films of SAM/Pt/ZnO/SiO_2. *Langmuir* **2008**, *24*, 14234−14244.

(21) Rai, P.; Kwak, W. K.; Yu, Y. T. Solvothermal Synthesis of ZnO Nanostructures and Their Morphology-Dependent Gas-Sensing Properties. *ACS Appl. Mater. Interfaces* **2013**, *5*, 3026−3032.

(22) Li, X. W.; Zhou, X.; Guo, H.; Wang, C.; Liu, J. Y.; Sun, P.; Liu, F. M.; Lu, G. Y. Design of Au@ZnO Yolk−Shell Nanospheres with Enhanced Gas Sensing Properties. *ACS Appl. Mater. Interfaces* **2014**, *6*, 18661−18667.

(23) Xia, Z. B.; Wang, Y. W.; Fang, Y. J.; Wan, Y. T.; Xia, W. W.; Sha, J. Understanding the Origin of Ferromagnetism in ZnO Porous Microspheres by Systematic Investigations of the Thermal Decomposition of $Zn_5(OH)_8Ac_2{\cdot}2H_2O$ to ZnO. *J. Phys. Chem. C* **2011**, *115*, 14576−14582.

(24) Shen, X. S.; Chen, L. Y.; Li, D. H.; Zhu, L. F.; Wang, H.; Liu, C. C.; Wang, Y.; Xiong, Q. H.; Chen, H. Y. Assembly of Colloidal Nanoparticles Directed by the Microstructures of Polycrystalline Ice. *ACS Nano* **2011**, *5*, 8426−8433.

(25) King, W. H. Piezoelectric Sorption Detector. *Anal. Chem.* **1964**, *36*, 1735−1739.

(26) Fan, G. K.; Wang, Y.; Hu, M.; Luo, Z. Y.; Li, G. Synthesis of Flowerlike Nano-SnO_2 and a Study of its Gas sensing Response. *Meas. Sci. Technol.* **2011**, *22*, 045203−045206.

(27) Zhu, G. X.; Liu, Y. J.; Xu, H.; Chen, Y.; Shen, X. P.; Xu, Z. Photochemical Deposition of Ag Nanocrystals on Hierarchical ZnO Microspheres and their Enhanced Gas-sensing Properties. *CrystEngComm* **2012**, *14*, 719−725.

(28) Polarz, S.; Strunk, J.; Ischenko, V.; Maurits, W. E.; Hinrichsen, O.; Muhler, M.; Driess, M. On the Role of Oxygen Defects in the Catalytic Performance of Zinc Oxide. *Angew. Chem., Int. Ed.* **2006**, *45*, 2965−2969.

(29) Chen, M.; Wang, X.; Yu, Y. H.; Pei, Z. L.; Bai, X. D.; Sun, C.; Huang, R. F.; Wen, L. S. X-ray Photoelectron Spectroscopy and Auger Electron Spectroscopy Studies of Al-doped ZnO Films. *Appl. Surf. Sci.* **2002**, *158*, 134−140.

(30) Islam, M. N.; Ghosh, T. B.; Chopra, K. L.; Acharya, H. N. XPS and X-ray Diffraction Studies of Aluminum-doped Zinc Oxide Transparent Conducting Films. *Thin Solid Films* **1996**, *280*, 20−25.

(31) Liu, D.; Lv, Y. H.; Zhang, M.; Liu, Y. F.; Zhu, Y. Y.; Zong, R. L.; Zhu, Y. F. Defect-related Photoluminescence and Photocatalytic Properties of Porous ZnO Nanosheets. *J. Mater. Chem. A* **2014**, *2*, 15377−15388.

(32) Djurišić, A. B.; Choy, W. C. H.; Roy, V. A. L.; Leung, Y. H.; Kwong, C. Y.; Cheah, K. W.; Gundu, R. T. K.; Chan, W. K.; Fei, L. H.; Surya, C. Photoluminescence and Electron Paramagnetic Resonance of ZnO Tetrapod Structures. *Adv. Funct. Mater.* **2004**, *14*, 856−864.

(33) Zhang, S. B.; Wei, S. H.; Zunger, A. Intrinsic n-type versus p-type Doping Asymmetry and the Defect Physics of ZnO. *Phys. Rev. B* **2001**, *63*, 075205.

(34) Galland, D.; Herve, A. Temperature Dependence of the ESR Spectrum of the Zinc Vacancy in ZnO. *Solid State Commun.* **1974**, *14*, 953−956.

DOI: 10.1021/acsami.5b01333
ACS Appl. Mater. Interfaces 2015, 7, 11824−11832

(35) Galland, D.; Herve, A. ESR Spectra of the Zinc Vacancy in ZnO. *Phys. Lett. A* **1970**, *33*, 1−2.
(36) Pöppl, A.; Völkel, G. ESR and Photo-ESR Investigations of Zinc Vacancies and Interstitial Oxygen Ions in Undoped ZnO Ceramics. *Phys. Status Solidi A* **1991**, *125*, 571−581.
(37) Wang, Z. L.; Lin, C. K.; Liu, X. M.; Li, G. Z.; Luo, Y.; Quan, Z. W.; Xiang, H. P.; Lin, J. Tunable Photoluminescent and Cathodoluminescent Properties of ZnO and ZnO:Zn Phosphors. *J. Phys. Chem. B* **2006**, *110*, 9469−9476.
(38) Deng, H.; Hossenlopp, J. M. Combined X-ray Diffraction and Diffuse Reflectance Analysis of Nanocrystalline Mixed Sn(II) and Sn(IV) Oxide Powders. *J. Phys. Chem. B* **2005**, *109*, 66−73.
(39) McLaren, A.; Solis, T. V.; Li, G. Q.; Tsang, S. C. Shape and Size Effects of ZnO Nanocrystals on Photocatalytic Activity. *J. Am. Chem. Soc.* **2009**, *131*, 12540−12541.
(40) Zeng, H. B.; Duan, G. T.; Li, Y.; Yang, S. K.; Xu, X. X.; Cai, W. P. Blue luminescence of ZnO Nanoparticles Based on Nonequilibrium Process: Defect Origins and Emission Controls. *Adv. Funct. Mater.* **2010**, *20*, 561−572.
(41) Meng, X. D.; Lin, B. X.; Fu, Z. X. Influence of CH_3COO^- on the Room Temperature Photoluminescence of ZnO Films Prepared by CVD. *J. Lumin.* **2007**, *126*, 203−206.
(42) Chen, D. M.; Wang, Z. H.; Ren, T. Z.; Ding, H.; Yao, W. Q.; Zong, R. L.; Zhu, Y. F. Influence of Defects on the Photocatalytic Activity of ZnO. *J. Phys. Chem. C* **2014**, *118*, 15300−15307.
(43) McLaren, A.; Solis, T. V.; Li, G. Q.; Tsang, S. C. Shape and Size Effects of ZnO Nanocrystals on Photocatalytic Activity. *J. Am. Chem. Soc.* **2009**, *131*, 12540−12541.
(44) Lee, J.; Shim, H. S.; Lee, M.; Song, J. K.; Lee, D. Size-Controlled Electron Transfer and Photocatalytic Activity of ZnO−Au Nanoparticle Composites. *J. Phys. Chem. Lett.* **2011**, *2*, 2840−2845.
(45) Zhu, C. Q.; Lu, B. A.; Su, Q.; Xie, E. Q.; Lan, W. A Simple Method for the Preparation of Hollow ZnO Nanospheres for Use as a High Performance Photocatalyst. *Nanoscale* **2012**, *4*, 3060−3064.
(46) Fageria, P.; Gangopadhyay, S.; Pande, S. Synthesis of ZnO/Au and ZnO/Ag Nanoparticles and Their Photocatalytic Application Using UV and Visible Light. *RSC Adv.* **2014**, *4*, 24962−24972.
(47) Xiang, Q.; Meng, G. F.; Zhao, H. B.; Zhang, Y.; Li, H.; Ma, W. J.; Xu, J. Q. Au Nanoparticle Modified WO_3 Nanorods with Their Enhanced Properties for Photocatalysis and Gas Sensing. *J. Phys. Chem. C* **2010**, *114*, 2049−2055.

DOI: 10.1021/acsami.5b01333
ACS Appl. Mater. Interfaces 2015, 7, 11824−11832